Nano Research 2018, 11(9): 4923–4930
https://doi.org/10.1007/s12274-018-2087-8
Research Article

ISSN 1998-0124
CN 11-5974/O4

Abnormal n-type doping effect in nitrogen-doped tungsten diselenide prepared by moderate ammonia plasma treatment

Zhepeng Jin, Zhi Cai, Xiaosong Chen, and Dacheng Wei (✉)

State Key Laboratory of Molecular Engineering of Polymers, Department of Macromolecular Science, Fudan University, Shanghai 200433, China

Received: 29 November 2017
Revised: 27 April 2018
Accepted: 7 May 2018

© Tsinghua University Press and Springer-Verlag GmbH Germany, part of Springer Nature 2018

KEYWORDS

nitrogen-doped,
tungsten diselenide,
n-type doping,
ammonia plasma,
anion vacancy

ABSTRACT

To facilitate potential applications of tungsten diselenide (WSe_2) in electronics, controllable doping is of great importance. As an industrially compatible technology, plasma treatment has been used to dope two-dimensional (2D) materials. However, owing to the strong etching effect in transition metal dichalcogenides (TMDCs), it is difficult to controllably dope 2D WSe_2 crystals by plasma. Herein, we develop a moderate ammonia plasma treatment method to prepare nitrogen-doped WSe_2 with controlled nitrogen content. Interestingly, Raman, photoluminescence, X-ray photoelectron spectroscopy, and electrical measurements reveal abnormal n-doping behavior of nitrogen-doped WSe_2, which is attributed to selenium anion vacancy introduced by hydrogen species in ammonia plasma. Nitrogen-doped WSe_2 with abnormal n-doping behavior has potential applications in future TMDCs-based electronics.

1 Introduction

In recent years, tungsten diselenide (WSe_2) has received considerable attention in photoelectronics and promises widespread potential applications [1–3]. WSe_2 is a two-dimensional (2D) semiconductor with unique properties, different from those of graphene. For instance, WSe_2 exhibits layer number-dependent band gap [4], strong light absorption properties (quantum efficiency: 45% for MoS_2 [5] and 80% for WSe_2 [6]), and high hole mobility [4]. Until now, WSe_2 has been regarded as one of the promising photoelectric or thermoelectric materials [7]. To fabricate WSe_2-based functional devices, controllable doping of WSe_2 is required. Doping with other elements is a promising way to achieve this goal. Up to now, molecular physisorption [8, 9] and chemisorption [10, 11] have been used to dope transition metal dichalcogenides (TMDCs) for electrical applications. For instance, Jo et al. realized conversion of WSe_2 channel from n-type to p-type via absorption of triphenylphosphine [8]. Fang et al. reported n-type doping of WSe_2 by utilizing

Address correspondence to weidc@fudan.edu.cn

NO_2 or potassium as a surface dopant [12, 13]. However, practical applications of molecular physisorption have received limited success, since the doping is normally unstable as a result of weak van der Waals interaction of the physical adsorption [9]. Currently, substitutional doping of TMDCs, in which dopant atoms are covalently bonded at vacancy sites [14], has been regarded as a promising alternative. Existing substitutional doping methods via high temperature treatment are complicated, time consuming, and lack controllability [13]. A simple and industry-compatible doping technology for substitutional doping of 2D WSe_2 for electronic devices is therefore still lacking.

Plasma treatment is a simple and industrially compatible technology, which has been used to dope and tailor electrical properties of various materials including graphene and MoS_2 [15, 16]. Owing to the strong etching effect of plasma, atomically thick TMDC materials tend to be etched or removed. Thus, plasma treatment is normally used to etch TMDC materials for obtaining pattern structures in lithography [10, 17, 18]. However controllable substitutional nitrogen doping of 2D WSe_2 by plasma treatment has remained elusive till now. In the present study, we develop a moderate ammonia (NH_3) plasma treatment method to prepare substitutional nitrogen-doped WSe_2, with higher simplicity and compatibility compared with existing methods. The nitrogen content after treatment reaches 5.7%, and the doping can be controlled by varying the power, treatment time, and pressure. Interestingly, Raman spectroscopy, photoluminescence (PL) spectroscopy, and X-ray photoelectron spectroscopy (XPS) characterizations as well as electrical measurements show an abnormal n-type doping effect in the nitrogen-doped WSe_2. This is different from previous results of nitrogen doping of the TMDCs (MoS_2) by remote nitrogen (N_2) plasma treatments wherein a p-type doping effect is observed [16, 19]. This difference is attributed to selenium anion vacancy introduced by hydrogen species in NH_3 plasma.

2 Experimental section

2.1 Materials

Pure NH_3 was purchased from the campus warehouse of Fudan University, Shanghai City, China. Tungsten oxide (WO_3; 99.9%) was purchased from Fluke, and selenium (Se) (≥ 99.5%) was purchased from Sigma-Aldrich. Heavily doped p-type silicon wafers with a 300 nm-thick layer of thermal SiO_2 were used as substrates.

2.2 Characterization

The samples were characterized by atomic force microscopy (AFM; Park XE7, tapping mode), XPS (Perkin-Elmer PHI 5300 with 250 W Mg Kα source, 1,253.6 eV), and Raman spectroscopy (HORIBA XploRA) at a laser excitation wavelength of 532 nm. The electrical properties were measured using a semiconductor device analyzer (Keysight B1500A) in vacuum. All the measurements were performed at 20–25 °C.

2.3 Preparation of substitutional nitrogen-doped WSe_2

The radio frequency plasma setup used for NH_3 plasma treatment mainly includes a plasma generator (13.56 MHz, K-mate, VERG-500RF) and a 2-inch quartz tube on it. A vacuum pump was used to evacuate the air from the quartz tube. The power supply was connected through the matching unit to a fourteen-turn inductance coil. The radius of the coil is 120 mm, while its length is 200 mm. The inductance coil is wound around the quartz tube. The WSe_2 sample was first annealed at 400 °C for 1 h under vacuum (1×10^{-5} Pa) to remove contamination absorbed during air exposure. The chamber pressure was maintained using a barometer. Pure NH_3 was introduced to the quartz tube in specific amounts using a flow controller. Then, the annealed WSe_2 surface was exposed to NH_3 plasma. The process was controlled by regulating the plasma power, processing time, and pressure.

3 Results and discussion

3.1 Substitutional nitrogen-doping by NH_3 plasma treatment

Large area 2D WSe_2 crystals were synthesized by chemical vapor deposition (CVD) [20]. The as-grown WSe_2 was loaded in the quartz tube, approximately

15 cm downstream to the plasma generator (Fig. 1(a)). In this work, we demonstrated a simple method to add nitrogen radicals into WSe_2. A variety of molecular and atomic radicals (H, N, NH, and NH_2) are produced by NH_3 plasma [15, 21, 22]. The results of the present study illustrate that NH_3 plasma has a strong dependence on the plasma power and treatment time, and the relationship between plasma power and treatment time can be described using three cases corresponding to three regions, as shown in Fig. 1(c). The marker i (40 W, 5 s), ii (8 W, 6 s), iii (10 W, 3 s), and iv (20 W, 5 s) in Fig. 1(c) represent the different processing conditions in the main text. The first case is etching. The AFM image of region 1 (Fig. 2(b)) shows the etched surface of the WSe_2 crystal after treatment with 40 W NH_3 plasma for 5 s (condition i). After the plasma treatment at this condition, the PL peaks (Fig. 2(c)) disappear, and the Raman peak intensity (Fig. 2(d)) decreases obviously, confirming the occurrence of etching or even removal of WSe_2 by plasma [23]. As no layer etching was detected after N_2 plasma exposure, we ascribe the etching to the creation of hydrogen species in the NH_3 plasma [16, 24, 25]. A similar etching of WSe_2 is observed after 10 W NH_3 plasma treatment for 20 s (Fig. S2(h) in the Electronic Supplementary Material (ESM)). The second case is doping. The AFM image of Region 2 (Fig. 2(f)) shows the surface of the WSe_2 crystal after plasma treatment at 8 W for 6 s (condition ii); there is no significant change in the surface condition compared to that of the pristine sample (Fig. 2(e)), indicating the absence of etching. A small N 1s peak is observed in the XPS spectrum

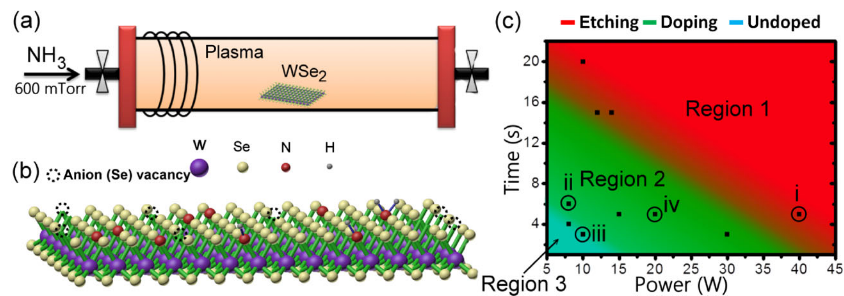

Figure 1 (a) Schematic illustration of the system for NH_3 plasma treatment. (b) Schematic illustration of the CVD-grown WSe_2 flake after treatment with NH_3 plasma. (c) Different conditions for preparing nitrogen-doped WSe_2 at the pressure of 600 mTorr.

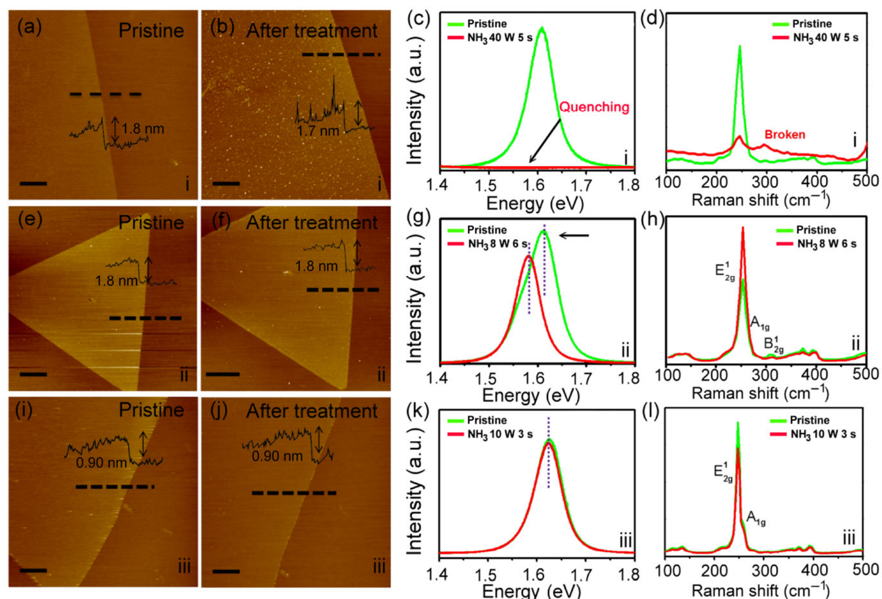

Figure 2 AFM images of WSe_2 ((a), (e), and (i)) before and ((b), (f), and (j)) after plasma treatment at conditions i (40 W, 5 s), ii (8 W, 6 s), and iii (10 W, 3 s), respectively, and the corresponding ((c), (g), and (k)) PL and ((d), (h), and (l)) Raman spectra. The scale bars represent 3 μm.

(Fig. 3(b)), and the nitrogen content is 1.1%, indicating the formation of nitrogen-doped WSe_2. The PL peak shows a red shift after NH_3 plasma treatment, manifesting that the Fermi energy is more close to the conduction band and indicating an n-type doping effect [26, 27], as shown in Fig. 2(g). The decrease in the PL intensity can be attributed to the n-type doping effect and reduced exciton lifetime [10, 24, 28, 29]. The Raman spectrum has no significant change (Fig. 2(h)), depicting that the lattices of WSe_2 remain intact after the NH_3 plasma treatment [24, 30]. The third case is absence of doping. In Region 3, the WSe_2 surface does not exhibit significant changes, as shown in Figs. 2(i) and 2(j) (condition iii).The PL (Fig. 2(k)) and the Raman spectra (Fig. 2(l)) show no significant changes after the plasma treatment, indicating that the crystal structure of WSe_2 is intact and no doping effect in this condition. A weak N 1s peak is observed in the XPS spectrum, and the nitrogen content is ~ 0.9%, as shown in Fig. 3(a), indicating that WSe_2 is doped with very little amount of nitrogen. According to the experimental results (black dots in Fig. 1(c)), the WSe_2 crystal is etched only when the value of plasma power multiplied by time is equal to or greater than ~ 200, and there is no obvious etching effect when the value is less than ~ 30. We concluded that WSe_2 is etched when the processing time is too long or the plasma power is too high, or no etching take place when the processing time is too short or the plasma power is too weak at 600 mTorr, as shown in Fig. 1(c). The experiment details are described in the ESM.

The N 1s XPS spectrum of WSe_2 after 20 W plasma treatment for 5 s (condition iv) is shown in Fig. 3(c), which consists of two peaks located at ~ 398 and ~ 400 eV, corresponding to N-W (from W-NH_x) and NH_x (NH_2, NH, and N) species [31, 32], respectively. The nitrogen content after treatment reaches 5.7% at this treatment condition. From the N 1s XPS spectrum of WSe_2 after 15 W NH_3 plasma treatment for 5 s (Fig. S3 in the ESM), the nitrogen content was found to be approximately about 1.2%. Figure 3(d) shows the nitrogen contents at different plasma treatment conditions. It is evident that the doping content can be controlled by varying the plasma power and the treatment time. Therefore, in the NH_3 plasma, the hydrogen radicals contribute to the etching of WSe_2

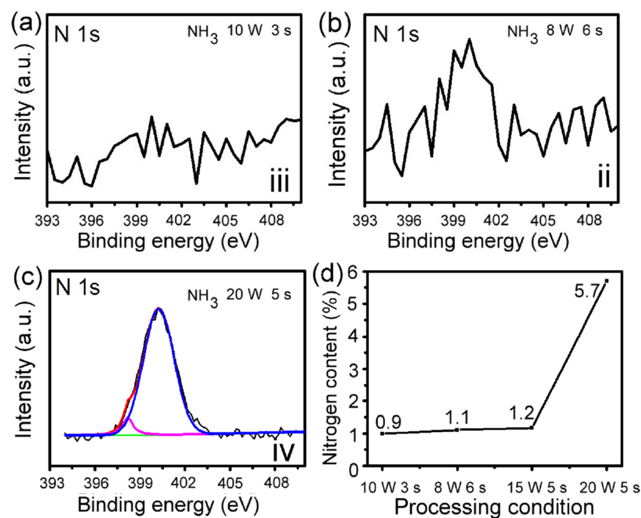

Figure 3 N 1s XPS spectra of WSe_2 after NH_3 plasma-treatment at (a) condition iii (10 W, 3 s), (b) condition ii (8 W, 6 s), and (c) condition iv (20 W, 5 s). (d) Nitrogen contents at different processing conditions.

surface, while the nitrogen (NH_2, NH, and N) radicals introduce nitrogen doping. Thus, nitrogen-doped WSe_2 is formed when there is a balance between etching and nitrogen doping (region 2 in Fig. 1(c)). The existence of nitrogen-doped WSe_2 is evident from the AFM image in Fig. 4(a) which shows slight cracks across the WSe_2 surface after 20 W plasma treatment for 5 s (condition iv) at 600 mTorr (white arrows in Fig. 4(a)). The slight cracks reflect ahexagonal-like symmetry. Interestingly, this phenomenon is similar to the work reported by Wallace et al in 2016. The depth of the cracks is ~ 0.4 nm, indicating that the cracks are formed only on the WSe_2 surface. These cracks may be formed from compressive strain as a result of

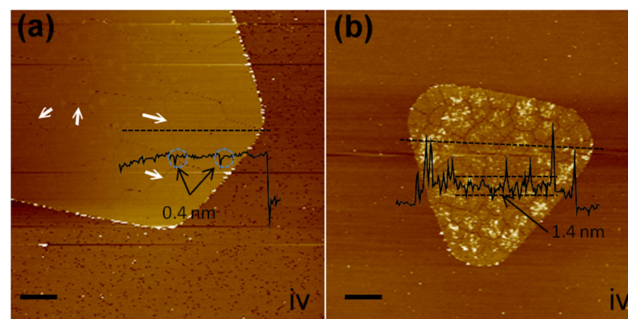

Figure 4 AFM images of WSe_2 after NH_3 plasma-treatment at (a) 600 and (b) 83 mTorr at conditions iv (20 W, 5 s). The line profile in black extends across a WSe_2 step, at which the heights of the cracks are shown in the AFM image. The scale bars represent 3 μm.

formation of W−N bonds owing to the smaller radius of nitrogen in comparison to that of selenium and a high nitrogen concentration at the surface [16]. Figure 4(b) depicts the AFM image of WSe_2 processed at 83 mTorr; the depth of the cracks is approximately ~ 1.4 nm. Although the WSe_2 surface is etched as a result of the impact of hydrogen species in the NH_3 plasma, increasing the power of plasma in this condition causes the development of cracks as a result of high nitrogen concentration, indicating the existence of nitrogen-doped WSe_2.

3.2 n-type doping effects by NH_3 plasma treatment

Figure 5 shows the Se 3d and the W 4f XPS spectra of plasma treated WSe_2 at conditions ii, iii, and iv. After 10 W plasma treatment for 3 s (condition iii), few vacancies are created in Region 3 by the hydrogen species in the NH_3 plasma, owing to the mild NH_3 plasma processing condition; thus, vacancy-induced doping can be ignored. The Se 3d (Fig. 5(a), pink line) and the W 4f (Fig. 5(d), pink line) peaks exhibit small red shifts, which can be attributed to p-doping [33]. As shown in Fig. S4 in the ESM, we ascribe this phenomenon to the small amount (~ 0.9%) of nitrogen dopant in WSe_2 [16]. However, after 8 W plasma treatment for 6 s (condition ii), the W 4f and the Se 3d peaks of WSe_2 corresponding to Region 2 are blue shifted by approximately 0.4 eV (from 32.2 to 32.6 eV and 34.4 to 34.8 eV) and 0.3 eV (from 54.7 to 55.0 eV), respectively, as shown in Figs. 5(b) and 5(e), which indicates n-type doping effect [8]. After 20 W plasma treatment for 5 s (condition iv), the Se 3d (Fig. 5(c)) and the W 4f (Fig. 5(f)) peaks are shifted by 0.4 eV (from 55.2 to 55.6 eV) and 0.5 eV (from 32.6 to 33.1 eV and 34.8 to 35.3 eV), respectively, revealing that the Fermi level of WSe_2 shifts to the conduction band owing to the n-doping effect [30, 34]. The variation in the XPS peaks with respect to the NH_3 plasma processing conditions is shown in Fig. S4 in the ESM. Generally, substitutional nitrogen-doped TMDCs show p-type doping behavior as a result of an increase in the acceptor doping level after nitrogen doping [16, 19]. The abnormal phenomenon observed in the present study can be attributed to the existence of (Se) anion vacancy caused by the hydrogen species in the NH_3 plasma [24].

To better understand the distribution of n-doping effects on the WSe_2 surface caused by the hydrogen species in the NH_3 plasma, we carried out Raman (249 cm^{-1}) and PL (1.62 eV, 1.57 eV) mapping of a WSe_2 sample (Figs. 6(b)–6(e)). The homogeneous color in Figs. 6(b) and 6(c) throughout the monolayer area confirms that the WSe_2 surface is uniform and that the crystal structure is intact before NH_3 plasma treatment [4]. After 20 W NH_3 plasma treatment for 5 s (condition iv), the Raman intensity at the edge of WSe_2 is weaker than that at the center (Fig. 6(d)), indicating that the hydrogen species in the NH_3 plasma caused superficial etching of the crystal structure at the edge of WSe_2. Figure 6(e) shows that the intensity

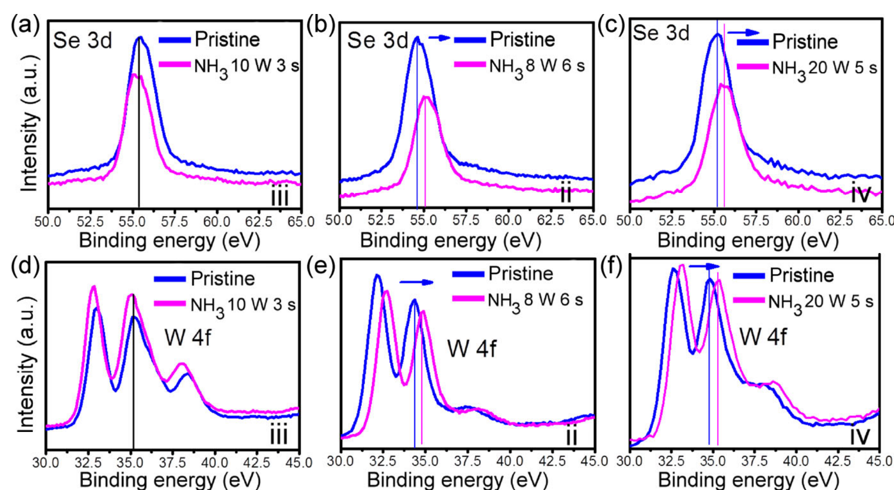

Figure 5 ((a), (b), and (c)) Se 3d, and ((d), (e), and (f)) W 4f XPS spectra of WSe_2 after plasma treatment at conditions iii (10 W, 3 s), ii (8 W, 6 s), and iv (20 W, 5 s), respectively.

of PL mapping (1.57 eV) at the edge of WSe_2 is stronger than that at the center, which display red shift at the edge of WSe_2 after NH_3 plasma treatment, indicating that n-doping effects of nitrogen-doped WSe_2 is easier to achieve at the edge than at the center of WSe_2. From the characterization results presented above, we can conclude that it is easier to form anion vacancy at the edge of the sample. By comparing the elemental ratios calculated by XPS before and after NH_3 plasma treatment, we can infer the loss of Se atoms with increased exposure to NH_3 plasma, as shown in Fig. S5 in the ESM. This indicates the existence of anion vacancy.

3.3 Electrical properties of WSe_2 after NH_3 plasma treatment

Back-gate top-contact field-effect transistors (FET) were fabricated on the 2D WSe_2 flakes. The device was fabricated by thermally depositing 30 nm Au electrodes on WSe_2 using a copper mesh as the mask. To avoid the doping effect caused by oxygen or moisture in air, the electronic measurements were performed in vacuum (1×10^{-5} Pa). Figure 7(a) shows the schematic of the WSe_2 FET before and after treatment. Before treatment, the WSe_2 FETs show typical p-type semiconductor characteristics, consistent with previous reports of untreated CVD grown WSe_2 [35, 36]. Firstly, the device was treated with 8 W NH_3 plasma for 6 s (condition ii). The transfer curves before and after treatment (Fig. 7(b) and Fig. S6(a) in the ESM) show that the ON/OFF ratios are approximately 10^6–10^7. The on current (I_{on}) decreases from 7.23×10^{-6} to 1.40×10^{-6} A. The threshold voltage (V_{th}) has a slight negative shift after NH_3 plasma treatment and the hole mobility decreases from 9.8 to 1.1 $cm^{-1}\cdot V^{-1}\cdot s^{-1}$, indicating the n-type doping effect of NH_3 plasma treatment [8, 28]. At the process condition of 20 W and 5 s (condition iv), the I_{on} remarkably decreases from 2.05×10^{-5} to 1.94×10^{-6} A (one order of magnitude reduction in the p-branch), the ON/OFF ratios decrease considerably, and the V_{th} shifts from −55.3 to −64.7 V, and the hole mobility decreases from 10.9 to 0.89 $cm^{-1}\cdot V^{-1}\cdot s^{-1}$, indicating a stronger n-doping effect at this condition, as displayed in Fig. 7(c) and Fig. S6(b) in the ESM. The carrier mobility (μ) can be deduced using the equation: $\mu = (L/WC_gV_{ds})(\Delta I_{ds}/\Delta V_g)$, where C_g is the gate capacitance per unit area (ca. 10 $nF\cdot cm^{-2}$), and L and W are the channel length and width, respectively. Owing to the strong Fermi level pinning at Au–WSe_2 interfaces [9], n-type characteristics were not observed in the FET. Figure S7 in the ESM displays the optical and the electrical properties of WSe_2 after 8 W plasma treatment for 4 s. The transfer curves show no significant change, including the values of I_{on} and V_{th} (Fig. S7(b) in the

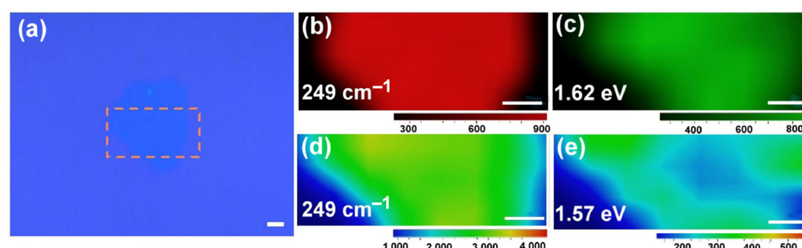

Figure 6 (a) Optical image of a WSe_2 monolayer. (b) Raman (249 cm^{-1}) and (c) PL (1.62 eV) mapping of WSe_2 before NH_3 plasma treatment. (d) Raman (249 cm^{-1}) and (e) PL (1.57 eV) spectra after 20 W plasma treatment for 5 s (condition iv). The scale bars are 10 μm.

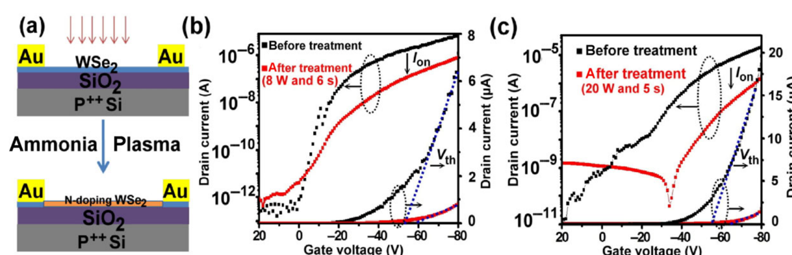

Figure 7 (a) Schematic illustration of the WSe_2 FET before and after ammonia treatment. I_{ds}–V_g characteristics of the WSe_2 FETs before and after plasma treatment at (b) 8 W, 6 s and (c) 20 W, 5 s ($V_{sd} = -2$ V).

ESM). According to the abnormal doping effect, the NH_3 plasma treatment realizes n-type doping and substitutional nitrogen doping simultaneously, which is difficult to be achieved by normal N_2 or H_2 plasma doping [16, 24].

4 Conclusions

In summary, we developed a moderate NH_3 plasma treatment method to produce nitrogen-doped WSe_2. This method realizes nondestructive and controllable nitrogen doping by tuning the plasma power, treatment time, and pressure. Corresponding characterization demonstrate the abnormal n-type doping effect of nitrogen-doped WSe_2, which is ascribed to anion vacancy-doping effect created by the hydrogen species in the ammonia plasma. This method also has the advantages of realizing nitrogen-doped WSe_2 by regulating the processing condition and controlling the doping type by etching action of hydrogen species simultaneously. Owing to its simplicity, scalability, as well as compatibility with current microelectronic industries, this method is valuable for both scientific research and practical applications of 2D materials in future electronic devices or circuits.

Acknowledgements

This work was supported by National Program for Thousand Young Talents of China, the National Natural Science Foundation of China (Nos. 51773041, 21603038 and 21544001), Shanghai Committee of Science and Technology in China (No. 18ZR1404900), and Fudan University.

Electronic Supplementary Material: Supplementary material (further details of the treatment method, AFM imaging, PL spectrum, Raman spectrum, statistics of XPS peaks shift and electrical properties) is available in the online version of this article at https://doi.org/10.1007/s12274-018-2087-8.

References

[1] Zhang Y. J.; Oka, T.; Suzuki, R.; Ye, J. T.; Iwasa, Y. Electrically switchable chiral light-emitting transistor. *Science* **2014**, *344*, 725–728.

[2] Kim, K.; Larentis, S.; Fallahazad, B.; Lee, K.; Xue, J. M.; Dillen, D. C.; Corbet, C. M.; Tutuc, E. Band alignment in WSe_2–graphene heterostructures. *ACS Nano* **2015**, *9*, 4527–4532.

[3] Ye, L.; Wang, P.; Luo, W. J.; Gong, F.; Liao, L.; Liu, T. D.; Tong, L.; Zang, J. F.; Xu, J. B.; Hu, W. D. Highly polarization sensitive infrared photodetector based on black phosphorus-on-WSe_2 photogate vertical heterostructure. *Nano Energy* **2017**, *37*, 53–60.

[4] Zhou, H. L.; Wang, C.; Shaw, J. C.; Cheng, R.; Chen, Y.; Huang, X. Q.; Liu, Y.; Weiss, N. O.; Lin, Z. Y.; Huang, Y. et al. Large area growth and electrical properties of p-type WSe_2 atomic layers. *Nano Lett.* **2015**, *15*, 709–713.

[5] Salehzadeh, O.; Tran, N. H.; Liu, X.; Shih, I.; Mi, Z. Exciton kinetics, quantum efficiency, and efficiency droop of monolayer MoS_2 light-emitting devices. *Nano Lett.* **2014**, *14*, 4125–4130.

[6] Massicotte, M.; Schmidt, P.; Vialla, F.; Schädler, K. G.; Reserbat-Plantey, A.; Watanabe, K.; Taniguchi, T.; Tielrooij, K. J.; Koppens, F. H. L. Picosecond photoresponse in van der Waals heterostructures. *Nat. Nanotechnol.* **2016**, *11*, 42–46.

[7] Chen, K. X.; Luo, Z. Y.; Mo, D. C.; Lyu, S. S. WSe_2 nanoribbons: New high-performance thermoelectric materials. *Phys. Chem. Chem. Phys.* **2016**, *18*, 16337–16344.

[8] Jo, S. H.; Kang, D. H.; Shim, J.; Jeon, J.; Jeon, M. H.; Yoo, G.; Kim, J.; Lee, J.; Yeom, G. Y.; Lee, S. et al. A high-performance WSe_2/h-BN photodetector using a triphenylphosphine (PPh_3)-based n-doping technique. *Adv. Mater.* **2016**, *28*, 4824–4831.

[9] Duclaux, L. Review of the doping of carbon nanotubes (multiwalled and single-walled). *Carbon* **2002**, *40*, 1751–1764.

[10] Sim, D. M.; Kim, M.; Yim, S.; Choi, M. J.; Choi, J.; Yoo, S.; Jung, Y. S. Controlled doping of vacancy-containing few-layer MoS_2 via highly stable thiol-based molecular chemisorption. *ACS Nano* **2015**, *9*, 12115–12123.

[11] Lei, S. D.; Wang, X. F.; Li, B.; Kang, J. H.; He, Y. M.; George, A.; Ge, L. H.; Gong, Y. J.; Dong, P.; Jin, Z. H. et al. Surface functionalization of two-dimensional metal chalcogenides by Lewis acid–base chemistry. *Nat. Nanotechnol.* **2016**, *11*, 465–471.

[12] Fang, H.; Tosun, M.; Srol, G.; Chang, T. C.; Takei, K.; Guo, J.; Javey, A. Degenerate n-doping of few-layer transition metal dichalcogenides by potassium. *Nano Lett.* **2013**, *13*, 1991–1995.

[13] Zhao, P. D.; Kiriya, D.; Zcatl, A.; Zhang, C. X.; Tosun, M.; Liu, Y. S.; Hettick, M.; Kang, J. S.; McDonnell, S.; Santosh, K. C. et al. Air stable p-doping of WSe_2 by covalent functionalization. *ACS Nano* **2014**, *8*, 10808–10814.

[14] Fang, H.; Chuang, S.; Chang, T. C.; Takei, K.; Takahashi, T.; Javey, A. High-performance single layered WSe_2 p-FETs with chemically doped contacts. *Nano Lett.* **2012**, *12*, 3788–3792.

[15] Lin, Y. C.; Lin, C. Y.; Chiu, P. W. Controllable graphene N-doping with ammonia plasma. *Appl. Phys. Lett.* **2010**, *96*, 133110.

[16] Azcatl, A.; Qin, X. Y.; Prakash, A.; Zhang, C. X.; Cheng, L. X.; Wang, Q. X.; Lu, N.; Kim, M. J.; Kim, J.; Cho, K. et al. Covalent nitrogen doping and compressive strain in MoS_2 by remote N_2 plasma exposure. *Nano Lett.* **2016**, *16*, 5437–5443.

[17] Chen, M. K.; Nam, H.; Wi, S. J.; Ji, L.; Ren, X.; Bian, L. F.; Lu, S. L.; Liang, X. G. Stable few-layer MoS_2 rectifying diodes formed by plasma-assisted doping. *Appl. Phys. Lett.* **2013**, *103*, 142110.

[18] Liu, Y. L.; Nan, H. Y.; Wu, X.; Pan, W.; Wang, W. H.; Bai, J.; Zhao, W. W.; Sun, L. T.; Wang, X. R.; Ni, Z. H. Layer-by-layer thinning of MoS_2 by plasma. *ACS Nano* **2013**, *7*, 4202–4209.

[19] Dolui, K.; Rungger, I.; Das Pemmaraju, C.; Sanvito, S. Possible doping strategies for MoS_2 monolayers: An *ab initio* study. *Phys. Rev. B* **2013**, *88*, 075420.

[20] Liu, B. L.; Fathi, M.; Chen, L.; Abbas, A.; Ma, Y. Q.; Zhou, C. W. Chemical vapor deposition growth of monolayer WSe_2 with tunable device characteristics and growth mechanism study. *ACS Nano* **2015**, *9*, 6119–6127.

[21] Narushima, K.; Yamashita, N.; Fukuoka, M.; Inagaki, N.; Isono, Y.; Islam, M. R. Surface modifications of polyester films by ammonia plasma. *Jpn. J. Appl. Phys.* **2007**, *46*, 4238.

[22] Milled, G. P.; Baird, J. K. Radio frequency plasma decomposition of ammonia: A comparison with radiation chemistry using the G value. *J. Phys. Chem.* **1993**, *97*, 10984–10988.

[23] Ma, Y. Q.; Liu, B. L.; Zhang, A. Y.; Chen, L.; Fathi, M.; Shen, C. F.; Abbas, A. N.; Ge, M. Y.; Mecklenburg, M.; Zhou, C. W. Reversible semiconducting-to-metallic phase transition in chemical vapor deposition grown monolayer WSe_2 and applications for devices. *ACS Nano* **2015**, *9*, 7383–7391.

[24] Tosun, M.; Chan, L.; Amani, M.; Roy, T.; Ahn, G. H.; Taheri, P.; Carraro, C.; Ager, J. W.; Maboudian, R.; Javey, A. Air-stable n-doping of WSe_2 by anion vacancy formation with mild plasma treatment. *ACS Nano* **2016**, *10*, 6853–6860.

[25] Xie, L. M.; Jiao, L. Y.; Dai, H. J. Selective etching of graphene edges by hydrogen plasma. *J. Am. Chem. Soc.* **2010**, *132*, 14751–14753.

[26] Chen, K.; Kiriya, D.; Hettick, M.; Tosun, M.; Ha, T. J.; Madhvapathy, S. R.; Desai, S.; Sachid, A.; Javey, A. Air stable n-doping of WSe_2 by silicon nitride thin films with tunable fixed charge density. *APL Mater.* **2014**, *2*, 092504.

[27] Hu, C.; Dong, D. D.; Yang, X. K.; Qiao, K. K.; Yang, D.; Deng, H.; Yuan, S. J.; Khan, J.; Lan, Y.; Song, H. S. et al. Synergistic effect of hybrid PbS quantum dots/2D-WSe_2 toward high performance and broadband phototransistors. *Adv. Funct. Mater.* **2017**, *27*, 1603605.

[28] Wu, Z. T.; Luo, Z. Z.; Shen, Y. T.; Zhao, W. W.; Wang, W. H.; Nan, H. Y.; Guo, X. T.; Sun, L. T.; Wang, X. R.; You, Y. M. et al. Defects as a factor limiting carrier mobility in WSe_2: A spectroscopic investigation. *Nano Res.* **2016**, *9*, 3622−3631.

[29] Mouri, S.; Miyauchi, Y.; Matsuda, K. Tunable photoluminescence of monolayer MoS_2 via chemical doping. *Nano Lett.* **2013**, *13*, 5944–5948.

[30] Crowther, A. C.; Ghassaei, A.; Jung, N.; Brus, L. E. Strong charge-transfer doping of 1 to 10 layer graphene by NO_2. *ACS Nano* **2012**, 6, 1865–1875.

[31] She, Y. G.; Mai, Y. W.; McBride, W. E.; Zhang, Q. C.; McKenzie, D. R. Structural properties and nitrogen-loss characteristics in sputtered tungsten nitride films. *Thin Solid Films* **2000**, 372, 257–264.

[32] Wei, D. C.; Liu, Y. Q.; Wang, Y.; Zhang, H. L.; Huang, L. P.; Yu, G. Synthesis of N-doped graphene by chemical vapor deposition and its electrical properties. *Nano Lett.* **2009**, *9*, 1752–1758.

[33] Nipane, A.; Karmakar, D.; Kaushik, N.; Karande, S.; Lodha, S. Few-layer MoS_2 p-type devices enabled by selective doping using low energy phosphorus implantation. *ACS Nano* **2016**, *10*, 2128–2137.

[34] Yang, L. M.; Majumdar, K.; Liu, H.; Du, Y. C.; Wu, H.; Hatzistergos, M.; Hung, P. Y.; Tieckelmann, R.; Tsai, W.; Hobbs, C. et al. Chloride molecular doping technique on 2D materials: WS_2 and MoS_2. *Nano Lett.* **2014**, *14*, 6275–6280.

[35] Liu, J. X.; Zeng, M. Q.; Wang, L. X.; Chen, Y. T.; Xing, Z.; Zhang, T.; Liu, Z.; Zuo, J. L.; Nan, F.; Mendes, R. G. et al. Ultrafast self-limited growth of strictly monolayer WSe_2 crystals. *Small* **2016**, *12*, 5741–5749.

[36] Chen, J. Y.; Liu, B.; Liu, Y. P.; Tang, W.; Nai, C. T.; Li, L. J.; Zheng, J.; Gao, L. B.; Zheng, Y.; Shin, H. S. et al. Chemical vapor deposition of large-sized hexagonal WSe_2 crystals on dielectric substrates. *Adv. Mater.* **2015**, *27*, 6722–6727.